J|A|C|S ARTICLES

Published on Web 11/10/2010

Visualizing and Tuning Thermodynamic Dispersion in Metalloprotein Monolayers

Amol Virendra Patil and Jason John Davis*

Physical and Theoretical Chemistry Laboratory, Department of Chemistry, University of Oxford, South Parks Road, Oxford OX1 3QZ, United Kingdom

Received August 4, 2010; E-mail: jason.davis@chem.ox.ac.uk

Abstract: In coupling the redox state of an adsorbed molecule to its spectral characteristics redox profiles can be directly imaged by means of far-field fluorescence. At suitable levels of dilution, on optically transparent electrode surfaces, reversible interfacial electron transfer processes can be followed pixel by pixel down to scales which approach the molecular. In mapping out switching potentials across a surface population, thermodynamic dispersion, related to variance in the orientation, electronic coupling, protein fold, electric field drop, and general surface order, can be quantified. The self-assembled monolayer buffering the protein from the underlying metallic electrode surface not only acts to tune electronic coupling between the two but also potentially provides a variable more easily segmented from other contributions to molecular dispersion. We have, specifically, considered the possibility that the supporting monolayer crystallinity is a significant contributor to the subsequently observed spread in half-wave potentials. We report here that this is indeed the case and that this spread diminishes from 17 to 12 mV for the blue copper protein azurin as the supporting alkanethiol layer crystallinity increases. The work herein, then, presents not only a direct determination of submonolayer scale variance in redox character but also a means of tuning this through gross surface and entirely standard chemical means.

Introduction

Metalloproteins participate in a number of fundamentally life sustaining biological processes such as photosynthesis and bioenergetic metabolism. An ability to analyze the electron transfer reactions that many of these metalloproteins participate in not only sheds light on important chemistry and natural molecular evolution but also commonly requires that we learn to communicate with these entities nondestructively. The redox centers of many biomolecules are deeply buried in a largely insulating protein fold, making reproducible electronic connectivity to a man-made surface experimentally challenging. Though mediator and/or interfacial recognition methods now exist which facilitate reasonable electron exchange, a more robust, interpretable, flexible, and potentially applicable format is generated by confining the biomolecule of interest to a surface (solution-based electrochemical analysis of macromolecules also inherently suffers from the significant limitations imposed by diffusion). Bioimmobilization also enables the resolution of faster electron transfer processes and requires typically fractions of a milligram of material which, in many cases, is valuable.[1−3] It also remains fundamental to the development of related or directly derived biosensors where interfacial immobilization potentially facilitates not only an environmentally flexible assay with minute (even disposable) quantities of the biocomponent but also multiplexing. A prerequisite of these interfacial analyses has been a thoughtful engineering of surface chemistry, ideally such that biological function and fold are retained while electronic coupling to the supporting electrode is maximized. Noncovalent approaches include physical adsorption, entrapment in gels or polymers, and hydrophobic, hydrophilic, and electrostatic interactions.[4−6] Covalent methods of immobilization can be site-specific through a single either naturally expressed or artificially induced functional group on the protein surface, and self-assembled monolayer (SAM) based electrode modifications have been optimized during the past decade or so to provide good levels of control over the bioimmobilization process and its homogeneity and orientational control.[7−9] Protocols for increasing surface loading and electronic coupling using carbon nanotubes and nanoparticles have also been developed.[10−12]

Though conceptually simpler, surface-confined electrochemical analyses almost always generate electrochemical responses which both deviate from the expected theoretical behavior and suffer from experiment-to-experiment variation. Such observa-

(1) Armstrong, F. A.; Heering, H. A.; Hirst, J. *Chem. Soc. Rev.* **1997**, *26*, 169.
(2) Hirst, J.; Duff, J. L. C.; Jameson, G. N. L.; Kemper, M. A.; Burgess, B. K.; Armstrong, F. A. *J. Am. Chem. Soc.* **1998**, *120*, 7085.
(3) Katz, E.; Willner, I. *Angew. Chem., Int. Ed.* **2004**, *43*, 6042.
(4) Kim, H.-J.; Lee, K.-S.; Won, M.-S.; Shim, Y.-B. *Langmuir* **2008**, *24*, 1087.
(5) Calvo, E. J.; Wolosiuk, A. *ChemPhysChem* **2004**, *5*, 235.
(6) Chi, Q.; Zhang, J.; Andersen, J. E. T.; Ulstrup, J. *J. Phys. Chem. B* **2001**, *105*, 4669.
(7) Azamian, B. R.; Davis, J. J.; Coleman, K. S.; Bagshaw, C. B.; Green, M. L. H. *J. Am. Chem. Soc.* **2002**, *124*, 12664.
(8) Astier, Y.; Bond, A. M.; Wijma, H. J.; Canters, G. W.; Hill, H. A. O.; Davis, J. J. *Electroanalysis* **2004**, *16*, 1155.
(9) Tominaga, M.; Soejima, K.; Manabu, M.; Taniguchi, I. *J. Electroanal. Chem.* **2005**, *579*, 51.
(10) Guiseppi-Elie, A.; Lei, C.; Baughman, R. H. *Nanotechnology* **2002**, *13*, 559.
(11) Katz, E.; Willner, I.; Wang, J. *Electroanalysis* **2004**, *16*, 19.
(12) Wang, J.; Li, M.; Shi, Z.; Li, N.; Gu, Z. *Electroanalysis* **2004**, *16*, 140.

10.1021/ja1065448

tions have been attributed to variant (and often undefined) contributions from electrode surface mechanical and electronic inhomogeneity, dispersion in molecular orientation, lateral interactions between redox sites, supporting monolayer variations, etc., although are rarely quantified or assigned with the support of experimental data.[13−18]

As with all "bulk" analyses, the faradaic responses obtained in these experiments are reflective of the average behavior of all molecules contributing to the sampling process; this is typically $10^{12}-10^{14}$ molecules in a bioelectrochemical experiment (depending upon the electrode area and surface coverage). The result is that an average distribution of properties is recorded (rather than the property distribution itself). As interest in the generation of derived "nanobio devices", composed of low numbers of biomolecules, grows, a detailed knowledge of molecular dispersion becomes not only fundamentally interesting but also fundamentally important.

To move redox analyses to a more molecularly refined scale, a number of approaches involving nanoelectrodes and proximal probe configurations have been tabled.[19−21] By combining the near-field imaging resolution of scanning tunneling (STM) or conductive probe atomic force (CPAFM) microscopy with electrochemical potential control, for example, it has been possible to obtain high-resolution conductance images of electrode-confined protein molecules and to carry out functional mapping based on current/voltage and conductance/surface potential relationships. Observations possible within such experimental formats generate a wealth of information about surface homogeneity, molecular conductance, redox site coupling to electrodes, and switching potentials at truly molecular scales.[22−27] Though they inherently contain information on dispersion present within any given molecular population and enable a direct "visualization" of redox potentials, these experiments and their subsequent theoretical analyses remain demanding.[21,28,29] Molecular scale information can be acquired in the far field by fluorescence microscopy with relative ease under a variety of controllable solution-phase conditions. The emission intensity and lifetime from surface-confined molecules can, for example, be measured and related to conformation dynamics.[30,31] At appropriate levels of surface dilution (on optically transparent matrixes) molecular scale information initially hidden in ensemble-based analyses is resolved.[32−35]

Azurin (from *Pseudomonas aeuruginosa*) is a blue single-copper protein with a molecular weight of 14 000. It acts as an electron transfer agent in the respiratory chain of denitrifying bacteria and has been extensively characterized.[36−40] The protein can be assembled directly and controllably on gold surfaces by either chemisorption of its solution exposed disulfide group or pairing of a hydrophobic area around the copper center with the methyl terminus of alkanethiol SAMs.[6,41−44] In its oxidized (Cu^{2+}) form the protein displays a strong ($\varepsilon = 5.6\ mM^{-1}\ cm^{-1}$) absorption in the 550−650 nm range, which corresponds to a $\pi-\pi^*$ transition of the Cu site, involving mainly the $d_{x^2-y^2}$ orbital on the Cu and a 3p orbital on the Cys112 sulfur. Upon reduction to Cu^+, there is negligible optical absorption in the 300−600 nm range. This redox-state-dependent absorbance has been used to modulate the fluorescence properties of a fluorescence resonance energy transfer (FRET) donor−acceptor pair, with the Cu site as the energy acceptor and an externally linked dye label as a fluorescent donor; an application of this principle to redox-state tracking of azurin molecules has been successfully demonstrated in solution and on suitably prepared electrode surfaces.[33,45,46] We have recently reported an extrapolation of this ability, termed fluorescence cyclic voltammetry (FCV), to the mapping of kinetic and thermodynamic dispersion within a population of electrode-confined protein molecules, with the resolution limit of a few hundred molecules, using a mathematically rigorous modified Butler−Volmer treatment.[35] Strikingly, electrochemical midpoint potentials are observed to span a Gaussian several tens of millivolts wide within a given population. This we attributed to a number of microenvironmental factors such as imperfections in the electrode surface, lateral protein interactions, variant structural perturbation and orientation at the surface, dispersion in the supporting monolayer quality, and associated redox site−electrode coupling.[15,17,47] Of these we have considered variations in the alkanethiol adlayer

(13) Cassidy, J.; Breen, W.; McGee, A.; McCormacx, T.; Lyons, M. E. G. *J. Electroanal. Chem.* **1992**, *333*, 313.
(14) Clark, R. A.; Bowden, E. F. *Langmuir* **1997**, *13*, 559.
(15) Rowe, G. K.; Carter, M. T.; Richardson, J. N.; Murray, R. W. *Langmuir* **1995**, *11*, 1797.
(16) Chidsey, C. E. D.; Bertozzi, C. R.; Putvinski, T. M.; Mujsce, A. M. *J. Am. Chem. Soc.* **1990**, *112*, 4301.
(17) Fawcett, W. R. *J. Electroanal. Chem.* **1994**, *378*, 117.
(18) Leger, C.; Jones, A. K.; Albracht, S. P. J.; Armstrong, F. A. *J. Phys. Chem. B* **2002**, *106*, 13058.
(19) Fan, F.-R. F.; Bard, A. J. *Science* **1995**, *267*, 871.
(20) Heller, I.; Kong, J.; Heering, H. A.; Williams, K. A.; Lemay, S. G.; Dekker, C. *Nano Lett.* **2004**, *5*, 137.
(21) Davis, J. J.; Morgan, D. A.; Wrathmell, C. L.; Axford, D. N.; Zhao, J.; Wang, N. *J. Mater. Chem.* **2005**, *15*, 2160.
(22) Davis, J. J.; Hill, H. A. O.; Bond, A. M. *Coord. Chem. Rev.* **2000**, *200−202*, 411.
(23) Davis, J. J.; Hill, H. A. O. *Chem. Commun.* **2002**, 393.
(24) Zhao, J.; Davis, J. J.; Sansom, M. S. P.; Hung, A. *J. Am. Chem. Soc.* **2004**, *126*, 5601.
(25) Chi, Q.; Farver, O.; Ulstrup, J. *Proc. Natl. Acad. Sci. U.S.A.* **2005**, *102*, 16203.
(26) Chi, Q.; Zhang, J.; Jensen, P. S.; Christensen, H. E. M.; Ulstrup, J. *Faraday Discuss. Chem. Soc.* **2006**, *131*, 181.
(27) Axford, D.; Davis, J. J.; Wang, N.; Wang, D.; Zhang, T.; Zhao, J.; Peters, B. *J. Phys. Chem. B* **2007**, *111*, 9062.
(28) Davis, J.; Peters, B.; Xi, W.; Axford, D. *Curr. Nanosci.* **2008**, *1*, 62.
(29) Davis, J. J.; Peters, B.; Xi, W.; Appel, J.; Kros, A.; Aartsma, T. J.; Stan., R.; Canters, G. W. *J. Phys. Chem. Lett.* **2010**, *10*, 1541.
(30) Weiss, S. *Nat. Struct. Biol.* **2000**, *7*, 724.
(31) Lu, H. P. *Acc. Chem. Res.* **2005**, *38*, 557.
(32) Xie, X. S.; Dunn, R. C. *Science* **1994**, *265*, 361.
(33) Davis, J. J.; Burgess, H.; Aartsma, T.; Canters, G. W. *J. Phys. Chem. B* **2006**, *110*, 20649.
(34) Lu, H. P.; Xie, X. S. *J. Phys. Chem B* **1997**, *101*, 2753.
(35) Salverda, J. M.; Patil, A. V.; Mizzon, G.; Kuznetsova, S.; Zauner, G.; Akkilic, N.; Canters, G. W.; Davis, J. J.; Heering, H. A.; Aartsma, T. J. *Angew. Chem., Int. Ed.* **2010**, *49*, 4776.
(36) Canters, G. W.; Hill, H. A. O.; Kitchen, N. A.; Adman, E. T. *J. Magn. Reson.* **1984**, *57*, 1.
(37) Gorren, A. C. F.; denBlaauwen, T.; Canters, G. W.; Hopper, D. J.; Duine, J. A. *FEBS Lett.* **1996**, *381*, 140.
(38) Kolczak, U.; Salgado, J.; Siegal, G.; Saraste, M.; Canters, G. W. *Biospectroscopy* **1999**, *5*, S19.
(39) Jeuken, L. J. C.; Ubbink, M.; Bitter, J. H.; Vliet, P. v.; Meyer-Klaucke, W.; Canters, G. W. *J. Mol. Biol.* **2000**, *299*, 737.
(40) Alessandrini, A.; Gerunda, M.; Canters, G. W.; Verbeet, M. P.; Facci, P. *Chem. Phys. Lett.* **2003**, *376*, 625.
(41) Gaigalas, A. K.; Niaura, G. *J. Colloid Interfac. Sci.* **1997**, *193*, 60.
(42) Chi, Q.; Zhang, J.; Nielsen, J. U.; Friis, E. P.; Chorkendorff, I.; Canters, G. W.; Andersen, J. E. T.; Ulstrup, J. *J. Am. Chem. Soc.* **2000**, *122*, 4047.
(43) Cavalleri, O.; Natale, C.; Stroppolo, M. E.; Relini, A.; Cosulich, E.; Thea, S.; Novi, M.; Gliozzi, A. *Phys. Chem. Chem. Phys.* **2000**, *2*, 4630.
(44) Fristrup, P.; Grubb, M.; Zhang, J.; Christensen, H. E. M.; Hansen, A. M.; Ulstrup, J. *J. Electroanal. Chem.* **2001**, *511*, 128.
(45) Schmauder, R.; Alagaratnam, S.; Chan, C.; Schmidt, T.; Canters, G. W.; Aartsma, T. J. *J. Biol. Inorg. Chem.* **2005**, *10*, 683.
(46) Kuznetsova, S.; Zauner, G.; Schmauder, R.; Mayboroda, O. A.; Deelder, A. M.; Aartsma, T. J.; Canters, G. W. *Anal. Biochem.* **2006**, *350*, 52.

crystallinity as a potential key, and tunable, determining factor in the protein environment (potentially affecting the orientation, solvation, field drop, and redox site−electrode electronic coupling). We report herein an application of FCV to an investigation of supporting monolayer effects on the subsequently observed thermodynamic dispersion in azurin voltammetry. Using a facile graphical method to analyze redox-triggered changes in molecular emission, a significant and stepwise decrease in the spread of half-wave potentials is observed with increasing alkanethiol chain length, a trend which neatly overlies contact angle data and directly highlights the effect of increasing film order on thermodynamic dispersion.

Experimental Procedures

Materials. All chemicals were reagent grade (Sigma-Aldrich) and were used without further purification. Deionized water (18.2 MΩ Millipore Ltd.) was used throughout.

SAM Formation. Optically transparent gold electrodes (OTEs) were fabricated by evaporating 10 nm of amorphous gold (rms roughness ∼1 nm), with a 2 nm chromium adhesion layer, on a glass coverslip (number 0, 0.08−0.11 mm thick, Menzel Glasser). Glassware, prior to use, was cleaned in freshly prepared piranha solution (a 10:3 mixture of sulfuric acid and hydrogen peroxide). *Caution: Piranha solution is a very strong oxidizing agent which will react violently with any organic material and must be handled with extreme care!* OTEs were dipped in piranha solution for 10 s, followed by a rinse in deionized water and absolute ethanol. They were then promptly transferred into 10 mM ethanolic solutions of *n*-alkanethiols ($n = 5$, 6, 7, 8, 9, and 11 for $CH_3(CH_2)_nSH$), where they were incubated overnight at room temperature. Prior to use the SAM-modified OTEs were rinsed in ethanol and deionized water.

Protein. Wild-type azurin protein labelled with Atto 655 (stock concentration 7 μM) was obtained from Prof. Canters, Leiden Institute of Chemistry, Leiden University, Leiden, The Netherlands. Stock was diluted to 1 μM in 200 mM phosphate buffer (pH 7.10) aliquots which were kept frozen at −80 °C. The Atto 655 labeling ratio, as determined by UV−vis spectroscopy, was found to be 1:5. Protein films were generated by exposure of SAM-modified OTEs to these solutions for 30 min at room temperature. Any nonadsorbed protein was removed by washing the surface repeatedly with 200 mM phosphate buffer.

Contact Angle Measurements. Contact angles were determined by the stationary sessile drop technique on an FTA1000B (First Ten Angstrom Inc.) goniometer at room temperature and ambient humidity. The contact angle was measured by forming a 20 μL drop at the end of a blunt-ended needle, lowering the drop to the surface, and removing the needle. The data were averaged over five readings taken at different locations on any given SAM-modified OTE.

Electrochemical Configuration. Electrochemical measurements were carried out in a modified single-compartment electrochemical cell, fabricated out of plexiglass (poly(methyl methacrylate)), consisting of functionalized OTE and SCE reference electrodes and a Pt gauze counter electrode with the electrolyte droplet confined by an O-ring. A LabVIEW algorithm recorded the time trace of the applied potential as applied by a μAutolab potentiostat (Eco Chemie, The Netherlands) controlled by GPES software. Cyclic voltammetry was carried out over a potential window of −0.15 to +0.2 V at a scan rate of 0.1 V/s, in degassed (nitrogen bubbled for at least 30 min) sodium phosphate buffer (pH 7.1, 200 mM).

Optical Configuration. The electrochemical cell was designed to allow simultaneous acquisition of electrochemical and optical data (see Figure SI1, Supporting Information). Fluorescence data were acquired with total internal reflection fluorescence microscopy (TIRF) with a Nikon TE2000-E microscope. The protein films were excited with a 633 nm CW laser (model 1135, 20 mW, JD Uniphase) through a 100× oil immersion objective. Emitted fluorescence light was filtered through a dichroic mirror (660 nm LP) and a 700/75 nm bandpass filter and was recorded with a 512 × 512 pixel CCD camera (Andor, Ireland) with an exposure time of 0.2 s.

Results and Discussion

Film Characteristics. The spontaneous formation of ordered alkanethiol monolayers on gold, due to the strong affinity of the sulfur head groups for this metal, has been extensively documented and known to proceed via a sequence of several structural phase transitions.[48−51] At lower coverages the SAM alkyl chains lie parallel to the supporting solid surface with a progressive transition to a standing up phase as molecular high coverage increases.[52,53] Common to all alkanethiols on Au(111) is the formation of an ordered SAM displaying a hexagonal $(\sqrt{3} \times \sqrt{3})R30°$ symmetry, corresponding to the adsorption of one thiol per three Au atoms. Long-chain alkanethiols display an additional modulation of the $(\sqrt{3} \times \sqrt{3})$ structure, yielding a *c* (4×2) superlattice with the same molecular concentration and have an associated tilt angle of ∼30° to the surface normal.[53−56] Within these films, it is well-known that the layer crystallinity and density increase with the alkyl chain length. Ellipsometric, Fourier transform infrared reflection−absorption spectroscopy (FT-IRRAS), and electrochemical analyses have, specifically, reported a progression toward lower order and packing density as the chain length falls, with the sharpest transition occurring between C_6 and C_{12} films.[55] Contact mode atomic force microscopy (AFM) studies have, additionally, suggested that longer chain SAMs are able to withstand greater tip−sample interactions, observations consistent with greater attractive chain−chain van der Waals interactions.[54,57]

Organic monolayers herein were prepared by immersing thin (∼100 Å) evaporated amorphous gold films (typically on 22 × 50 mm glass coverslips) in dilute ethanolic solutions of alkanethiols. Room temperature wetting angle measurements show an expected increase in surface hydrophobicity with increasing chain length (Figure SI2, Supporting Information). The structural integrity (presence of defects) of these SAM films was further probed with a ferrocenemethanol electrochemical redox probe, which exploits the fact that a long-chain alkanethiol acts as a physical barrier preventing redox probe molecules from closely approaching the gold electrode surface, where progressively decreasing faradic and capacitive current responses with chain length are observed (Figure SI3, Supporting Information). Additional electrodesorption studies (in nitrogen-deaerated 0.2 M KOH) confirmed a cathodic progression of stripping potential

(47) Clark, R. A.; Bowden, E. F. *Langmuir* **1997**, *13*, 559.
(48) Bain, C. D.; Troughton, E. B.; Tao, Y.; Evall, J.; Whitesides, G. M.; Nuzzon, R. G. *J. Am. Chem. Soc.* **1989**, *111*, 321.
(49) Bain, C. D.; Whitesides, G. M. *J. Am. Chem. Soc.* **1988**, *110*, 6560.
(50) Kawasaki, M.; Sato, T.; Tanaka, T.; Takao, K. *Langmuir* **2000**, *16*, 1719.
(51) Vericat, C.; Vela, M. E.; Benitez, G. A.; Gago, J. A. M.; Torrelles, X.; Salvarezza, R. C. *J. Phys.: Condens. Matter* **2006**, *18*, R867.
(52) Poirier, G. E. *Langmuir* **1999**, *15*, 1167.
(53) Godin, M.; Williams, P. J.; Tabard-Cossa, V.; Laroche, O.; Beaulieu, L. Y.; Lennox, R. B.; Gruetter, P. *Langmuir* **2004**, *20*, 7090.
(54) Fukuma, T.; Kobayashi, K.; Horiuchi, T.; Yamada, H.; Matsushige, K. *Appl. Phys. A: Mater. Sci. Process.* **2001**, *72*, S109.
(55) Porter, M. D.; Bright, T. B.; Allara, D. L.; Chidsey, C. E. D. *J. Am. Chem. Soc.* **1987**, *109*, 3559.
(56) Dubois, L. H.; Zegarski, B. R.; Nuzzo, R. G. *J. Chem. Phys.* **1993**, *98*, 678.
(57) Alves, C. A.; Smith, E. L.; Porter, M. D. *J. Am. Chem. Soc.* **1992**, *114*, 1222.

with increasing carbon chain length (Figure SI4, Supporting Information) (chronocoulometric analyses of surface coverage ranging from 1.5×10^{14} to 3×10^{14} molecules/cm^2 [58−60]). These observations uniformly confirm the expected trend to greater film order with an increase in the number of methylenes.[48,49,55] [Although the underlying microscopic gold roughness of our (amorphous) electrodes is expected to contribute to the SAM crystallinity, especially where lateral van der Waals interactions are minimal (short alkyl chains),[61−65] the comparative trends in contact angle presented (Figure SI2) are fully consistent with those reported on single-crystal surfaces.[66,67]]

The structural, spectroscopic, and electron transfer characteristics of azurin have been extensively studied in solution,[68−72] and the role of the protein's hydrophobic surface region in its natural electron transfer and binding events is well established.[73−75] Azurin is known to physisorb on methyl-terminating alkanethiol monolayers through this same hydrophobic patch such that the copper redox center faces the underlying electrode surface.[25,26] The predominance of hydrophobic forces in this protein−surface association has been confirmed and, indeed, energetically estimated.[6,41] The electron transfer kinetics, tunneling, and topographic characteristics of these interfaces have been previously detailed.[6,33,35,44] Films of the protein on thiol SAMs have, specifically, been characterized by surface-enhanced Raman spectroscopy (SERS), electroreflectance, and an extensive barrage of voltammetric methods and at molecular (near-field imaging) scales by us and others.[6,21,26,29,41,43,44,76] Protein orientational control has been confirmed in experiments where the electron transfer kinetics to underlying gold electrode surfaces have been mapped across a range of film thicknesses.[6]

Electroactive molecular densities of the fluorophore-labeled protein (Figure 1) determined herein were observed to be largely independent of the thiol adlayer, broadly in line with previous reports [$(1-4) \times 10^{12}$ molecules/cm^2] and indicative of submonolayer to monolayer coverage. In prior work we have noted significant molecular clustering within these films at such coverages.[35]

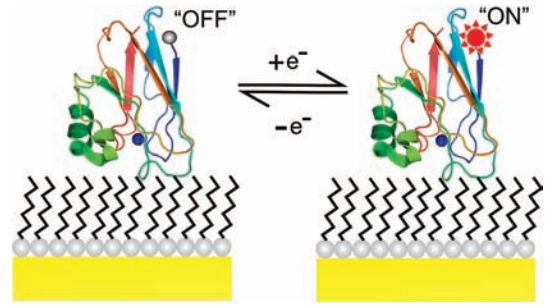

Figure 1. Schematic representation of dye-labeled *P. aeruginosa* azurin immobilized on an alkanethiol monolayer. The protein is orientated through a hydrophobic patch on its surface in a manner which facilitates robust electronic coupling between the copper site (blue sphere) and the underlying electrode. The copper site is also optically (FRET) coupled to an externally appended organic fluorophore (gray or red). In switching the copper oxidation state, emission from the latter is modulated ("on" for Cu^+, "off" for Cu^{2+}) and provides a means of directly imaging electron transfer processes pixel by pixel on suitably prepared electrodes.

The application of an appropriate triangular voltage waveform (−0.15 to +0.2 V at a scan rate of 0.1 V/s) to these surfaces enables, through total internal reflection mode imaging, redox state changes to be tracked as a series of fluorescence intensity time-elapsed snapshots (0.2 s of exposure time, 0.077 s frame transfer time). Earlier investigations have shown that solution-based redox titrations of labeled azurin have a switching ratio (defined as $1 - (F_{min}/F_{max})$) of about 80%, a value that agrees with the distance between the dye and copper site, based on the crystal structure of the wild-type azurin.[33] The average switching ratio obtained herein for the N-terminus-appended-fluorophore-labeled protein is about 30−50%, indicating quenching (which is expected to be associated with configurations in which redox coupling is most facile)[33] caused by the presence of a gold surface approximately 4 nm from the fluorophore and the impact of this on the mean "on" state intensity. The observed variations in switching ratio and brightness within fluorescence images, additionally, hint at heterogeneity in the sample (data not shown).

Temporal data associated with molecular clusters within these optical data were manually segmented with a macro in ImageJ (available at http://rsb.info.nih.gov/ij, developed by Wayne Rasband, National Institutes of Health, Bethesda, MD). The segmented clusters, from hereon referred to as regions of interest (ROIs), were 6 × 6 pixels on average (1 square pixel = 106 × 106 nm^2 as determined by graticule calibration). Time traces of a typical ROI (Figure 2) show a periodic variation of fluorescence intensity amplitude overlaid on a progressive negative slope of photobleaching (which varies from ROI to ROI). [A few protein clusters show non-FRET modulations in emission which we have previously attributed to electric field induced modulations in fluorophore−electrode interaction (typical switching magnitude of 1−10%).[33,35]] Only those ROIs showing a reversible, symmetrical behavior at asymptotic applied potential values were selected for further analysis (typically 75−90% selected). This temporal behavior selection criterion, *applied without knowledge of the corresponding applied potential value*, eliminates selection bias. Raw data, containing time traces of up to 200 ROIs, were further analyzed using a home-written MatLab algorithm (R2008b, MathWorks).

(58) Hobara, D.; Sasaki, T.; Imabayashi, S.-i.; Kakiuchi, T. *Langmuir* **1999**, *15*, 5073.
(59) Vela, M. E.; Martin, H.; Vericat, C.; Andreasen, G.; Hernandez Creus, A.; Salvarezza, R. C. *J. Phys. Chem. B* **2000**, *104*, 11878.
(60) Hatchett, D. W.; Uibel, R. H.; Stevenson, K. J.; Harris, J. M.; White, H. S. *J. Am. Chem. Soc.* **1998**, *120*, 1062.
(61) Creager, S. E.; Hockett, L. A.; Rowe, G. K. *Langmuir* **1992**, *8*, 854.
(62) Guo, L.-H.; Facci, J. S.; McLendon, G.; Mosher, R. *Langmuir* **1994**, *10*, 4588.
(63) Hou, Z.; Dante, S.; Abbott, N. L.; Stroeve, P. *Langmuir* **1999**, *15*, 3011.
(64) Hou, Z.; Abbott, N. L.; Stroeve, P. *Langmuir* **1998**, *14*, 3287.
(65) Losic, D.; Shapter, J. G.; Gooding, J. J. *Langmuir* **2001**, *17*, 3307.
(66) Troughton, E. B.; Bain, C. D.; Whitesides, G. M.; Nuzzo, R. G.; Allara, D. L.; Porter, M. D. *Langmuir* **1988**, *4*, 365.
(67) Laibinis, P. E.; Whitesides, G. M.; Allara, D. L.; Tao, Y. T.; Parikh, A. N.; Nuzzo, R. G. *J. Am. Chem. Soc.* **1991**, *113*, 7152.
(68) Farver, O.; Pecht, I. *J. Am. Chem. Soc.* **1992**, *114*, 5764.
(69) Gray, H. B.; Winkler, J. R. *Annu. Rev. Biochem.* **1996**, *65*, 537.
(70) Winkler, J. R.; Gray, H. B. *J. Biol. Inorg. Chem.* **1997**, *2*, 399.
(71) Nar, H.; Messerschmidt, A.; Huber, R.; Kamp, M. v. d.; Canters, G. W. *J. Mol. Biol.* **1991**, *221*, 765.
(72) Nar, H.; Messerschmidt, A.; Huber, R.; van de Kamp, M.; Canters, G. W. *FEBS Lett.* **1992**, *306*, 119.
(73) Farver, O.; Blatt, Y.; Pecht, I. *Biochemistry* **1982**, *21*, 3556.
(74) Van de Kamp, M.; Floris, R.; Hali, F. C.; Canters, G. W. *J. Am. Chem. Soc.* **1990**, *112*, 907.
(75) van de Kamp, M.; Silvestrini, M. C.; Brunori, M.; Van Beeumen, J.; Hali, F. C.; Canters, G. W. *Eur. J. Biochem.* **1990**, *194*, 109.
(76) Andolfi, L.; Bruce, D.; Cannistraro, S.; Canters, G. W.; Davis, J. J.; Hill, H. A. O.; Crozier, J.; Verbeet, M. P.; Wrathmell, C. L.; Astier, Y. *J. Electroanal. Chem.* **2004**, *565*, 21.

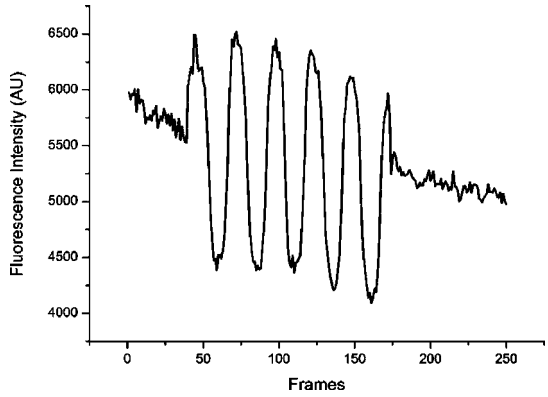

Figure 2. Time traces of an ROI (6 pixels × 6 pixels encompassing approximately 1200 molecules) showing FRET-gated emission of Atto 655-labeled protein clusters on a decanethiol-modified OTE in response to an applied voltage train (0.2 V/s). The system is initially held at 0 V and then conditioned at −0.2 V for 2 s, following which a triangular potential waveform (−0.2 to +0.15 V) is applied and terminated at 0 V (vs SCE).

Photobleaching, which is temporal in nature, potentially complicates data analysis as the fluorescence intensity and its change are the principal metrics in all analyses.

This was accordingly compensated for within each individual time trace using a MatLab algorithm which fitted the outliers with an exponential decay function. Subsequent to this photobleaching compensation each time trace was individually normalized using a min−max normalization, wherein each trace containing n intensity frames (I_n) was mapped onto new normalized intensity (I_n') values according to

$$I_n' = \frac{I_n - \min(I)}{\max(I) - \min(I)} \tag{1}$$

This algorithm also calculated the applied surface potential values associated with each image frame, by aligning the applied potential wave (utilizing LabVIEW-recorded time stamps) and image time traces (time stamps as recorded by the camera). An overlay of emission and potential plots confirms, as previously reported, that surface potentials cathodic of the bulk electrochemical half-wave remove the high extinction charge transfer transition, switch off FRET, and enable radiative decay of the externally appended fluorophore.[33,46]

By plotting the normalized fluorescence intensity as a function of the applied potential, it is possible to generate "optical voltammograms", conceptually equivalent to classical cyclic voltammograms (obtained for surface-confined redox systems). It is useful to note at this point that, unlike the classical cyclic voltammograms where the current signal decreases on either side of the half-wave potential (as the redox-active state responsible for current generation is depleted in the film), optical voltammograms achieve a steady state at asymptotic values since the fluorophores that are in a specific switch state (on or off) remain fixed at overpotentials, resulting in sigmoidal behavior (Figure 3). In utilizing the fact that the fluorescence emission intensity reflects the number of molecules in a reduced form, we can define the "optical peak potential" (E_p) as the potential at which the rate of change of the fluorescence intensity is maximum. As shown in Figure 3, E_p can be found by fitting

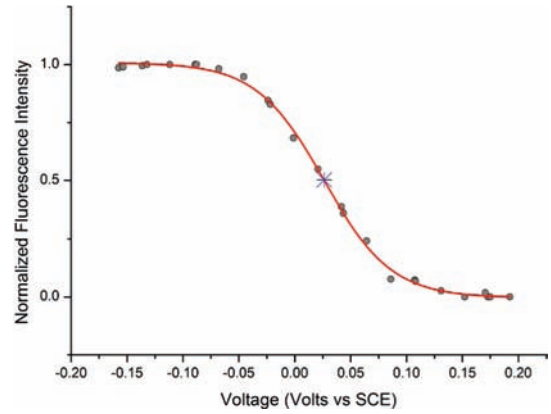

Figure 3. Fit of the Boltzmann sigmoidal (eq 2) (red line) to the normalized fluorescence intensity vs applied potential (backward sweep direction) for a single ROI (6 pixels × 6 pixels) on decanethiol. Each circular point represents the fluorescence intensity as captured in a frame (exposure time of 0.2 s) for a single ROI (approximately 1200 molecules). The optically determined peak potential "E_p" (blue star) is the calculated value from the sigmoidal fit at which the rate of change of fluorescence is maximum (E_p = 0.026 V).

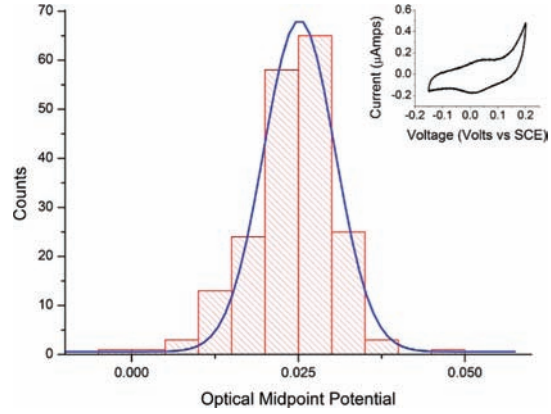

Figure 4. Gaussian fit to the optically determined midpoint potential for 6.1×10^6 molecules (across 194 ROIs) on a decanethiol-modified OTE at an applied scan rate of 0.2 V/s. The Gaussian is centered on 25.16 mV (with an fwhm of 12.6 mV), which is within 3 mV of the bulk midpoint potential (surface coverage of 1.5×10^{12} molecules/cm^2) as calculated from the associated voltammetric response (inset).

the normalized fluorescence intensity (I_f) trend for half-potential sweep to a Boltzmann sigmoidal equation, given by

$$I_f = I_{f,min} + \frac{I_{f,max} - I_{f,min}}{1 + \exp\left(\frac{E - E_p}{dE}\right)} \tag{2}$$

Thus, by taking an average of optical peak potentials for a forward and backward sweep, the optical midpoint potential (OMP) can be calculated. Poor fits, which were indicated by high values of reduced χ^2 and nonsensical values of E_p (>0.2 and <−0.15) were discarded from further consideration (typically 1−4% in any one sample). Figure 4 shows the dispersion in the optically determined midpoint potential for ∼6.1×10^6 molecules on a decanethiol-modified OTE. The fitted Gaussian distribution has a mean value of 25.16 mV with a standard deviation of 12.6 mV. This dispersion, obtained purely graphically, lies in good agreement with a recently published report where emission potential trends were subject to a more vigorous theoretical analysis.[35]

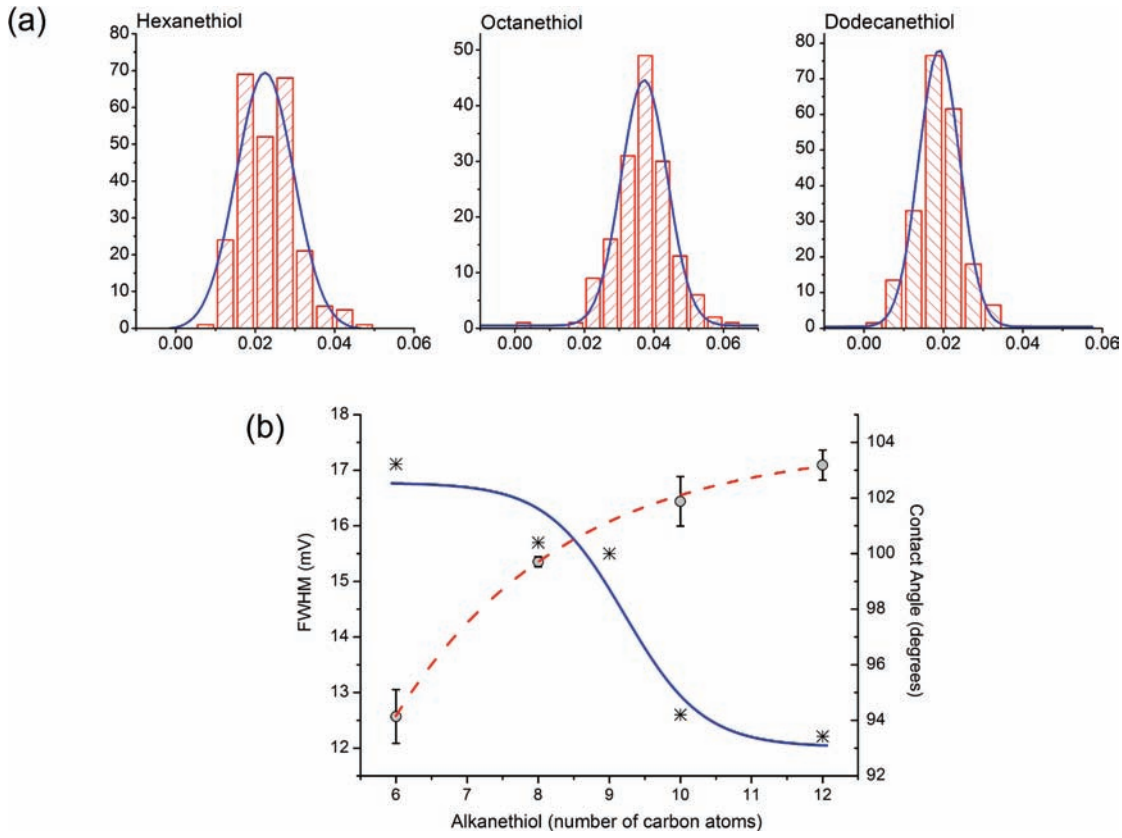

Figure 5. (a) Comparison of Gaussian fits to optically determined midpoint potentials for wild-type azurin molecules tagged with Atto 655 on hexanethiol (fwhm = 17.11 mV), octanethiol (fwhm = 15.64 mV), and dodecanethiol (fwhm = 12.15 mV) modified OTEs, showing a decrease of approximately 30% in the fwhm across the increasing chain length. (b) Each data point (black star) represents the fwhm of a Gaussian fit to an OMP histogram. Each OMP histogram (containing at least 200 ROIs) was generated by sampling different locations on multiple samples of each surface. The sigmoidal trend (blue line) in the decrease of fwhm (with increasing alkanethiol chain length) lies nicely complementarily to acquired contact angle data (where each gray circle represents the average of five measurements at different locations for each alkanethiol-modified gold electrode surface), where the expected progression to increasing hydrophobic character (red dashed line) with increasing chain length is observed, the sharpest change being between hexanethiol and decanethiol films.

Significantly, an equivalent analysis (i.e., multiple ROIs at different locations across a range of identically prepared samples where random variations in experimental conditions such as variation in the gold surface/localized SAM defects should be averaged out) across a range of supporting alkanethiol monolayers indicates that dispersion in OMP consistently falls sigmoidally as the carbon chain length is varied (Figure 5a,b). The electrochemical half wave potential, specifically, spans almost a 30% (or 10 mV) greater range with the shortest (hexanethiol) thiol layer than with the longest (dodecanethiol) (Figure 5a). This ability to "tune" the exhibited thermodynamic dispersion is observed to be consistent across many tens of carefully prepared samples across a range of layer modifications. At the higher limit of SAM crystallinity, i.e., dodecanethiol (although the crystallinity may be higher for yet longer chain lengths, one will lose the ability to drive electron transfer to/from the protein),[6] the observed thermodynamic dispersion spans a 12 mV range presumably reflective of remaining microenvironmental variance, protein orientation, protein fold, and fitting errors (generated while analyzing the fluorescence−voltage traces).

Conclusions

In 1977 both Eddowes and Hill[77] and Yeh and Kuwana[78] presented methods to prevent denaturation of proteins at the electrode surface. This led the way to the direct observation of electron exchange between an electrode and proteins and of enzymatic turnover as a function of the applied surface potential.[79] Bioelectrochemical analyses were further refined with the discovery that many redox proteins can be nondestructively immobilized on electrode surfaces in such a way that their redox-active centers undergo fast interfacial electron exchange. The removal of diffusion limitations enables a direct analysis of intrinsic electron transfer characteristics and may further facilitate fast rates of electron exchange if the electronic coupling between the protein prosthetic group and the supporting man-made electrode can be made strong.

Though proteins can be productively coupled to gold electrode surfaces through either cysteine residues introduced by site-directed mutagenesis,[76] or solution-exposed disulfide bridges,[80] this is not a common approach, and bare metallic surfaces generally cause loss of the native protein fold. A surface prefunctionalization is, therefore, often carried out prior to bioimmobilization (or indeed diffusive bioelectrochemistry). In the three decades that have followed the initial reports on 4,4-bipyridyl-modified gold, a large number of charged, charge neutral, and chelating electrode modifications have been

(77) Eddowes, M. J.; Hill, H. A. O. *J. Chem. Soc., Chem. Commun.* **1977**, 771.

(78) Yeh, P.; Kuwan, T. *Chem. Lett.* **1977**, 1145.

(79) Armstrong, F. A.; Hill, H. A. O.; Walton, N. J. *Acc. Chem. Res.* **1988**, *21*, 407.

(80) Davis, J. J.; Halliwell, C. M.; Hill, H. A. O.; Canters, G. W.; van Amsterdam, M. C.; Verbeet, M. P. *New J. Chem.* **1998**, *22*, 1119.

utilized.[8,81−83,22,84−86] The spatial separation between the redox site and electrode unavoidably generated through such modifications has a now well-understood impact on the kinetics of electron transfer in both the medium and short chain length regimes.[6,87−89] Though these interfacial methods have been undoubtedly powerful in shedding light on protein structure, conformational fluctuation, natural bioelectronic design, and enzyme activity, for example, and also in educating researchers in optimizing communication with (and ultimately utilization of) biological molecules, surface-confined bioelectrochemical analyses commonly generate responses which show both variance and deviation from ideal theoretical behavior. Though distributions in surface bioredox properties have been referred to or indeed assumed for some time,[18,90−92] and a significant part of the "nonidealities" reported are likely to be ascribable to directly associated nonidealities within the film structure, the methods by which this can be directly resolved are limited.[93−97] By appending a FRET-coupled organic fluorophore to the exterior of a redox-active metalloprotein and optically engaging the molecules through a transparent electrode in a TIRF configuration, electron transfer signatures can be resolved at molecular scales (demonstrably down to a few tens of molecules),[35] an ability which enables electrochemical thermodynamic dispersion to be quantified across a library of modified gold electrode surfaces.

The association of a protein with electrode surfaces is a complex function of surface chemistry, pH, hydration, electrostatics, ionic strength, and hydrophobic interactions. The subsequently observed electron transfer characteristics at these interfaces reflect not only this potential complexity but also the related variance in orientation, electronic coupling, protein fold, electric field drop, etc. There are, then, a number of closely related contributors one may seek to segment (some only with considerable difficulty). We have demonstrated herein not only a facile, fully graphical method of quantifying electrochemical dispersion but also that the supporting monolayer crystallinity is a key controllable variable that can, alone, dramatically affect the dispersion in protein electron transfer characteristics. Further work is under way to deconvolute additional contributors.

Acknowledgment. We acknowledge Professors Gerard Canters and Thijs Aartsma of the University of Leiden for productive and supportive discussions and financial support from the European Community through the EdRox Network (Contract MRTN-CT-2006-035649).

Supporting Information Available: Schematic representation of the electrochemical TIRF setup, contact angle measurements, redox probe analyses, and alkanethiol layer reductive stripping potentials. This material is available free of charge via the Internet at http://pubs.acs.org.

JA1065448

(81) Chattopadhyay, K.; Mazumdar, S. *Bioelectrochemistry* **2001**, *53*, 17.
(82) Paul, A.; watson, R. M.; Lund, P.; Xing, Y.; Burke, K.; He, Y.; Borguet, E.; Achim, C.; Waldeck, D. H. *J. Phys. Chem. C* **2008**, *112*, 7233.
(83) Yue, H.; Khoshtariya, D.; Waldeck, D. H.; Grochol, J.; Hildebrandt, P.; Murgida, D. H. *J. Phys. Chem. B* **2006**, *110*, 19906.
(84) Zhang, Z.; Nasser, A.-E.; Lu, Z.; Schenkman, J. B.; Rusling, J. F. *J. Chem. Soc., Faraday Trans.* **1997**, *93*, 1769.
(85) Hess, C. R.; Juda, G. A.; Dooley, D. M.; Amii, R. N.; Hill, M. G.; Winkler, J. R.; Gray, H. B. *J. Am. Chem. Soc.* **2003**, *125*, 7156.
(86) Johnson, D. L.; Martin, L. L. *J. Am. Chem. Soc.* **2005**, *127*, 2018.
(87) Petrovic, J.; Clark, R. A.; Yue, H.; Waldeck, D. H.; Bowden, E. F. *Langmuir* **2005**, *21*, 6308.
(88) Avila, A.; Gregory, B. W.; Niki, K.; Cotton, T. M. *J. Phys. Chem. B* **2000**, *104*, 2759.
(89) Song, S.; Clark, R. A.; Bowden, E. F. *J. Phys. Chem.* **1993**, *97*, 6564.
(90) Albery, W. J.; Boutelle, M. G.; Colby, P. J.; Hillman, A. R. *J. Electroanal. Chem.* **1982**, *133*, 135.
(91) Fleming, B. D.; Barlow, N. L.; Zhang, J.; Bond, A. M.; Armstrong, F. A. *Anal. Chem.* **2006**, *78*, 2948.
(92) Lee, C.; Bond, A. M. *Anal. Chem.* **2009**, *81*, 584.
(93) Palacios, R. E.; Fan, F. F.; Grey, J. K.; Suk, J.; Bard, A. J.; Barbara, P. F. *Nat. Mater.* **2007**, *6*, 680.
(94) Palacios, R. E.; Fan, F.-R. F.; Bard, A. J.; Barbara, P. F. *J. Am. Chem. Soc.* **2006**, *128*, 9028.
(95) Jiang, R.; Anson, F. C. *J. Electroanal. Chem.* **1991**, *305*, 171.
(96) Williams, C. G.; Edwards, M. A.; Colley, A. L.; Macpherson, J. V.; Unwin, P. R. *Anal. Chem.* **2009**, *81*, 2486.
(97) Feng, J.-J.; Murgida, D. H.; Kuhlmann, U.; Utesch, T.; Mroginski, M. A.; Hildebrandt, P.; Weidinger, I. M. *J. Phys. Chem. B* **2008**, *112*, 15202.